Computational symmetry hierarchy of time-reversal-even and -odd spin Hall conductivity tensors in altermagnets

Dameul Jeong[1], Seoung-Hun Kang[1,2,3*], Young-Kyun Kwon[1,2*]

[1]Department of Physics and Research Institute for Basic Sciences, Kyung Hee University, Kyungheedae-ro 26, Seoul, 02447, Korea.
[2]Department of Information Display, Kyung Hee University, Kyungheedae-ro 26, Seoul, 02447, Korea.
[3]Research Center for Technology Commercialization, Korea Institute of Science and Technology Information (KISTI), Hoegiro 66, Seoul, 02456, Korea.

*Corresponding author(s). E-mail(s): shkang@kisti.re.kr; ykkwon@khu.ac.kr;
Contributing authors: wjdekamf@khu.ac.kr;

S1 Crystal Structure

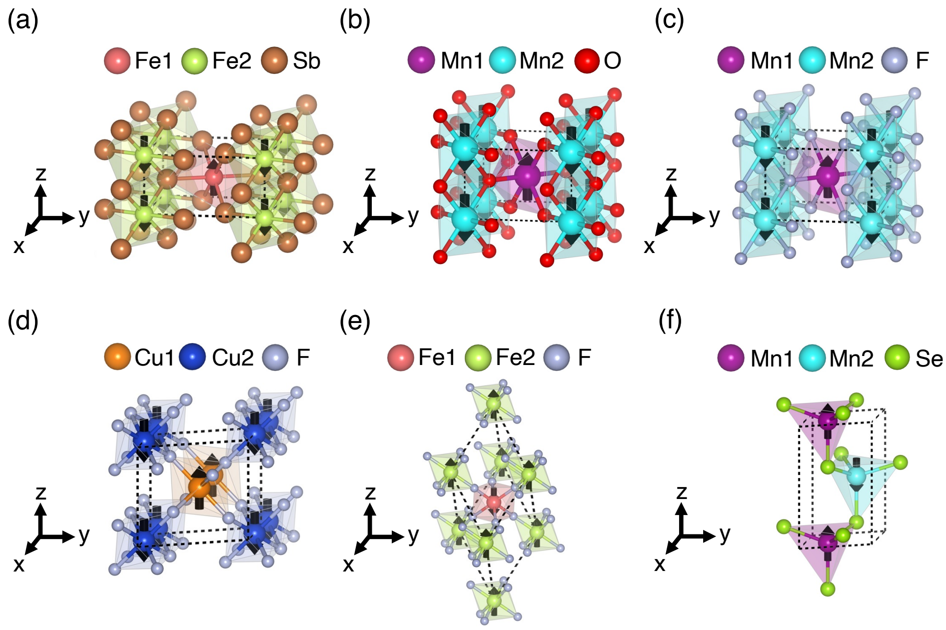

Fig. S1 Crystal structures of representative altermagnetic materials considered in this work. (a) $FeSb_2$, (b) MnO_2, (c) MnF_2, (d) CuF_2, (e) FeF_3, and (f) MnSe. Distinct magnetic sublattices are indicated by different colors for the transition-metal ions, while anions are shown in lighter tones. The dashed black lines denote the conventional crystallographic unit cells, and the coordinate axes are shown for reference. The corresponding Laue groups are $FeSb_2$ (mmm), MnO_2 (4/mmm), MnF_2 (4/mmm), CuF_2 (2/m), FeF_3 ($\bar{3}$m), and MnSe (6mm).

The crystallographic structures and lattice parameters of all materials investigated in this work are summarized below and visualized in Fig. S1. Fig. S1(a) shows the orthorhombic crystal structure of $FeSb_2$, characterized by lattice constants $a_1 = 5.82$ Å, $a_2 = 6.57$ Å, and $a_3 = 3.25$ Å. Figs. S1(b) and S1(c) display the tetragonal structures of MnO_2 and MnF_2, respectively, with lattice constants $a_1 = a_2 = 4.50$ Å and $a_3 = 2.95$ Å for MnO_2, and $a_1 = a_2 = 5.15$ Å and $a_3 = 3.38$ Å for MnF_2.

Fig. S1(d) presents the monoclinic crystal structure of CuF_2, with lattice constants $a_1 = 3.41$ Å, $a_2 = 5.37$ Å, and $a_3 = 4.62$ Å, where the angle between a_1 and a_2 is 120.69°. The rhombohedral structure of FeF_3 is shown in Fig. S1(e), characterized by a lattice constant $a = 5.45$ Å and a rhombohedral angle of 58.64°. Finally, Fig. S1(f) shows the hexagonal structure of MnSe, with lattice constants $a = 4.28$ Å and $a_3 = 6.87$ Å.

In Fig. S1, conventional crystallographic unit cells are indicated by dashed black lines, and the crystallographic axes are shown for reference. Distinct transition-metal sites that form different magnetic sublattices are highlighted by different colors, while ligand atoms are depicted with smaller spheres. This figure provides a direct real-space visualization of the lattice symmetries underlying the symmetry analysis presented in the main text and clarifies how the different crystal systems—orthorhombic, tetragonal, monoclinic, rhombohedral, and hexagonal—determine the associated Laue-group symmetries and the symmetry-allowed tensor components discussed in this work.

S2 Allowed SHC tensor Components

S2.A Symmetry-analysis framework

The spin Hall conductivity (SHC) tensor σ_{ij}^{k} is a rank-three response tensor that relates the spin current J_i^k to the applied electric field E_j through $J_i^k = \sigma_{ij}^k E_j$. Here, the index i denotes the flow direction of the spin current and the index j denotes the electric-field direction. Both are polar-vector indices, because the velocity/current direction and the electric field transform in the same way as an ordinary displacement vector under spatial operations. By contrast, the spin-polarization index k is an axial-vector index, because spin transforms as an angular momentum. Equivalently, spin has the same transformation character as $\boldsymbol{r}\times\boldsymbol{p}$, the cross product of two polar vectors.

Under a point-group operation g, we denote by $D(g)$ the corresponding 3×3 orthogonal representation matrix acting on the polar vectors in Cartesian coordinates, $v_i \mapsto D(g)_{ii'}\, v_{i'}$. Thus, $\det D(g) = +1$ for proper rotations and $\det D(g) = -1$ for improper operations such as mirrors, inversion, and rotoinversions. While a polar vector transforms only with $D(g)$, an axial vector transforms with an additional determinant factor, $S_k \mapsto \det D(g)\, D(g)_{kk'}\, S_{k'}$. Combining the two polar indices i, j and the one axial spin index k, the SHC tensor transforms as

$$\sigma_{ij}^{k} \;\longmapsto\; \det D(g)\, D(g)_{ii'}\, D(g)_{kk'}\, D(g)_{jj'}\, \sigma_{i'j'}^{k'}, \tag{S1}$$

with summation over the primed indices implied. The factor $\det D(g)$ therefore accounts for the axial character of the spin index, whereas the polar indices i and j transform without any additional determinant factor.

For a magnetic crystal, the magnetic point group can be written as $M = H \cup \mathcal{T}A$, where H is the unitary subgroup and $\mathcal{T}A$ is the antiunitary coset when antiunitary operations are present. Here, A denotes the set of spatial operations g that appear in the antiunitary operations $\mathcal{T}g$. For type-I groups, $A = \varnothing$ and $H = M$. Following the $\mathcal{T}$-parity decomposition of the spin conductivity tensor into Fermi-sea ($\mathcal{T}$-even) and Fermi-surface ($\mathcal{T}$-odd) contributions, a tensor component is symmetry-allowed only if the full magnetic operation acting on it leaves it invariant.

For $g \in H$, the full magnetic operation is the spatial operation g itself. For $g \in A$, the full magnetic operation is the antiunitary operation $\mathcal{T}g$, not g alone. The spatial part g transforms the tensor indices according to Eq. (S1), whereas $\mathcal{T}$ contributes only the time-reversal parity of the response. Therefore, the $\mathcal{T}$-even contribution satisfies

$$g: \quad \sigma_{ij}^{\mathrm{sea},k} \mapsto \left(g\cdot\sigma^{\mathrm{sea}}\right)_{ij}^{k} = \sigma_{ij}^{\mathrm{sea},k}, \qquad g \in H, \tag{S2a}$$

$$\mathcal{T}g: \quad \sigma_{ij}^{\mathrm{sea},k} \mapsto +\left(g\cdot\sigma^{\mathrm{sea}}\right)_{ij}^{k} = \sigma_{ij}^{\mathrm{sea},k}, \qquad g \in A, \tag{S2b}$$

whereas the $\mathcal{T}$-odd contribution satisfies

$$g: \quad \sigma_{ij}^{\mathrm{surf},k} \mapsto \left(g\cdot\sigma^{\mathrm{surf}}\right)_{ij}^{k} = \sigma_{ij}^{\mathrm{surf},k}, \qquad g \in H, \tag{S3a}$$

$$\mathcal{T}g: \quad \sigma_{ij}^{\mathrm{surf},k} \mapsto -\left(g\cdot\sigma^{\mathrm{surf}}\right)_{ij}^{k} = \sigma_{ij}^{\mathrm{surf},k}, \qquad g \in A. \tag{S3b}$$

Here, $(g\cdot\sigma)$ denotes only the spatial tensor transformation defined in Eq. (S1). The final equality to σ in Eqs. (S2)–(S3) is the invariance condition required for the tensor component to survive the magnetic symmetry. The minus sign in the A coset for σ^{surf} reflects the odd time-reversal parity of the Fermi-surface contribution. Thus, in the antiunitary coset, a $\mathcal{T}$-odd tensor component can survive only when the spatial part g compensates the sign change from time reversal. These constraints are imposed on the full rank-three tensor and generate the complete set of symmetry-allowed components, including their symmetric pieces and the relations among them.

S2.B Sublattice classification for altermagnets

For an altermagnetic ground state with two collinear magnetic sublattices A ($\uparrow$) and B ($\downarrow$) aligned along $\hat{\boldsymbol{z}}$, each parent operation g falls into one of the four cases listed in Table S1, determined by its action on σ_z and on the sublattice labels.

Table S1 Assignment of a parent operation g to the unitary subgroup H or the antiunitary coset $\mathcal{T}\cdot A$ of the magnetic point group of an altermagnet with $\boldsymbol{M} \parallel \pm\hat{\boldsymbol{z}}$.

Action on σ_z	Action on sublattice	MPG assignment
preserve	preserve ($A\to A$, $B\to B$)	H (unitary)
preserve	exchange ($A\leftrightarrow B$)	$\mathcal{T}\cdot A$ (antiunitary)
flip	preserve	$\mathcal{T}\cdot A$ (antiunitary)
flip	exchange	H (unitary)

S2.C Numerical implementation and validation

For numerical symmetry analysis, we first rewrite the SHC tensor as a finite-dimensional vector. Before imposing symmetry constraints, the rank-three tensor σ_{ij}^{k} has $3\times 3\times 3 = 27$ components. We gather these components into a single vector $\vec{\sigma}$ using the linear index

$$\ell = 9k + 3i + j,$$

where $i, j, k = 0, 1, 2$ corresponds to x, y, z, respectively. With this convention, the nine components with fixed spin polarization $k = x$ come first, followed by those with $k = y$ and $k = z$.

Each symmetry operation g is then represented by its induced 27×27 matrix $\rho_\sigma(g)$ acting on the vectorized SHC tensor. The entries of $\rho_\sigma(g)$ are obtained directly from the tensor transformation rule in Eq. (S1). Thus, $\rho_\sigma(g)$ simply encodes how the operation g permutes, relates, or changes the signs of the 27 tensor components.

A symmetry-allowed tensor must satisfy all symmetric constraints of the magnetic point group. For a unitary operation $g \in H$, the tensor must remain unchanged after applying g, which gives

$$\vec{\sigma} = \rho_\sigma(g)\vec{\sigma}.$$

For an antiunitary operation $\mathcal{T}g$ with $g \in A$, the constraint depends on the time-reversal parity of the response. The $\mathcal{T}$-even channel is invariant under time reversal, whereas the $\mathcal{T}$-odd channel changes sign. Therefore, the allowed tensor space is obtained from the linear constraints

$$\left[\rho_\sigma(g) - \mathbf{I}_{27}\right]\vec{\sigma} = 0, \qquad g \in H, \tag{S4a}$$

$$\left[\rho_\sigma(g) \mp \mathbf{I}_{27}\right]\vec{\sigma} = 0, \qquad g \in A. \tag{S4b}$$

Here, the upper sign applies to the $\mathcal{T}$-even channel and the lower sign applies to the $\mathcal{T}$-odd channel in Eq. (S4b). The matrix $\mathbf{I}_{27}$ denotes the 27×27 identity matrix in the vector space of the SHC tensor components.

The resulting linear constraints are solved numerically using singular-value decomposition. This procedure determines which tensor components are forced to vanish, which surviving components are related by symmetry, and how many independent tensor parameters remain.

To validate the implementation, we first consider the nonmagnetic limit. In this limit, no antiunitary magnetic operation is present. Therefore, we set $A = \emptyset$ and take H as the full crystallographic point group. The symmetry analysis then reduces to the ordinary crystallographic selection rule for the SHC tensor. The resulting tensor forms agree with the exhaustive nonmagnetic classification of Roy *et al.* [S1], as summarized in Table S2. Clearly, a nonmagnetic crystal is described by the gray magnetic group $G + \mathcal{T}G$. In this gray limit, the $\mathcal{T}$-even SHC sector is constrained in the same way as by the crystallographic group G, whereas the $\mathcal{T}$-odd sector is forbidden by pure time-reversal symmetry. Therefore, the comparison in Table S2 should be understood as a benchmark of the $\mathcal{T}$-even crystallographic selection rules implemented in the present framework.

Table S2 Benchmark of the present framework against the nonmagnetic SHC classification of Roy *et al.* [S1] for selected Laue classes. Entries are given as allowed components / linearly independent components.

Laue class	Roy *et al.* [S1]	This work
$\bar{3}$	21 / 9	21 / 9
$\bar{3}m$	10 / 4	10 / 4
$4/mmm$	6 / 3	6 / 3
$6/mmm$	6 / 3	6 / 3

S2.D Application to representative altermagnetic materials

Applying Eqs. (S1)–(S3) together with the sublattice classification of Table S1 to the magnetic point groups of the six altermagnets considered here, we obtain the symmetry-allowed σ^{sea} and σ^{surf} tensors summarized in the following pages. For each material the structure of the allowed-component matrices, the number of independent parameters, and the explicit linear relations among components are reported.

$FeSb_2$

$\mathcal{T}$-even

$$\begin{array}{ccc} \sigma^x & \sigma^y & \sigma^z \\ \begin{pmatrix} 0 & 0 & 0 \\ 0 & 0 & \sigma^x_{yz} \\ 0 & \sigma^x_{zy} & 0 \end{pmatrix} & \begin{pmatrix} 0 & 0 & \sigma^y_{xz} \\ 0 & 0 & 0 \\ \sigma^y_{zx} & 0 & 0 \end{pmatrix} & \begin{pmatrix} 0 & \sigma^z_{xy} & 0 \\ \sigma^z_{yx} & 0 & 0 \\ 0 & 0 & 0 \end{pmatrix} \end{array}$$

6 components, 6 independent

$FeSb_2$

$\mathcal{T}$-odd

$$\begin{array}{ccc} \sigma^x & \sigma^y & \sigma^z \\ \begin{pmatrix} 0 & 0 & 0 \\ 0 & 0 & \sigma^x_{yz} \\ 0 & \sigma^x_{zy} & 0 \end{pmatrix} & \begin{pmatrix} 0 & 0 & \sigma^y_{xz} \\ 0 & 0 & 0 \\ \sigma^y_{zx} & 0 & 0 \end{pmatrix} & \begin{pmatrix} 0 & \sigma^z_{xy} & 0 \\ \sigma^z_{yx} & 0 & 0 \\ 0 & 0 & 0 \end{pmatrix} \end{array}$$

6 components, 6 independent

MnO_2 & MnF_2

$\mathcal{T}$-even

$$\begin{array}{ccc} \sigma^x & \sigma^y & \sigma^z \\ \begin{pmatrix} 0 & 0 & 0 \\ 0 & 0 & \sigma^x_{yz} \\ 0 & \sigma^x_{zy} & 0 \end{pmatrix} & \begin{pmatrix} 0 & 0 & \sigma^y_{xz} \\ 0 & 0 & 0 \\ \sigma^y_{zx} & 0 & 0 \end{pmatrix} & \begin{pmatrix} 0 & \sigma^z_{xy} & 0 \\ \sigma^z_{yx} & 0 & 0 \\ 0 & 0 & 0 \end{pmatrix} \end{array}$$

6 components, 3 independent

$$\sigma^z_{xy} = -\sigma^z_{yx}, \sigma^y_{zx} = -\sigma^x_{zy}, \sigma^x_{yz} = -\sigma^y_{xz}$$

MnO_2 & MnF_2

$\mathcal{T}$-odd

$$\begin{array}{ccc} \sigma^x & \sigma^y & \sigma^z \\ \begin{pmatrix} 0 & 0 & 0 \\ 0 & 0 & \sigma^x_{yz} \\ 0 & \sigma^x_{zy} & 0 \end{pmatrix} & \begin{pmatrix} 0 & 0 & \sigma^y_{xz} \\ 0 & 0 & 0 \\ \sigma^y_{zx} & 0 & 0 \end{pmatrix} & \begin{pmatrix} 0 & \sigma^z_{xy} & 0 \\ \sigma^z_{yx} & 0 & 0 \\ 0 & 0 & 0 \end{pmatrix} \end{array}$$

6 components, 3 independent

$$\sigma^z_{xy} = \sigma^z_{yx}, \sigma^y_{zx} = \sigma^x_{zy}, \sigma^x_{yz} = \sigma^y_{xz}$$

CuF_2

$\mathcal{T}$-even

$$\begin{array}{ccc} \sigma^x & \sigma^y & \sigma^z \\ \begin{pmatrix} 0 & \sigma^x_{xy} & 0 \\ \sigma^x_{yx} & 0 & \sigma^x_{yz} \\ 0 & \sigma^x_{zy} & 0 \end{pmatrix} & \begin{pmatrix} \sigma^y_{xx} & 0 & \sigma^y_{xz} \\ 0 & \sigma^y_{yy} & 0 \\ \sigma^y_{zx} & 0 & \sigma^y_{zz} \end{pmatrix} & \begin{pmatrix} 0 & \sigma^z_{xy} & 0 \\ \sigma^z_{yx} & 0 & \sigma^z_{yz} \\ 0 & \sigma^z_{zy} & 0 \end{pmatrix} \end{array}$$

13 components, 13 independent

CuF_2

$\mathcal{T}$-odd

$$\begin{array}{ccc} \sigma^x & \sigma^y & \sigma^z \\ \begin{pmatrix} \sigma^x_{xx} & 0 & \sigma^x_{xz} \\ 0 & \sigma^x_{yy} & 0 \\ \sigma^x_{zx} & 0 & \sigma^x_{zz} \end{pmatrix} & \begin{pmatrix} 0 & \sigma^y_{xy} & 0 \\ \sigma^y_{yx} & 0 & \sigma^y_{yz} \\ 0 & \sigma^y_{zy} & 0 \end{pmatrix} & \begin{pmatrix} \sigma^z_{xx} & 0 & \sigma^z_{xz} \\ 0 & \sigma^z_{yy} & 0 \\ \sigma^z_{zx} & 0 & \sigma^z_{zz} \end{pmatrix} \end{array}$$

14 components, 14 independent

FeF$_3$
$\mathcal{T}$-even

$$\overset{\sigma^x}{\begin{pmatrix} \sigma^x_{xx} & 0 & 0 \\ 0 & \sigma^x_{yy} & \sigma^x_{yz} \\ 0 & \sigma^x_{zy} & 0 \end{pmatrix}} \overset{\sigma^y}{\begin{pmatrix} 0 & \sigma^y_{xy} & \sigma^y_{xz} \\ \sigma^y_{yx} & 0 & 0 \\ \sigma^y_{zx} & 0 & 0 \end{pmatrix}} \overset{\sigma^z}{\begin{pmatrix} 0 & \sigma^z_{xy} & 0 \\ \sigma^z_{yx} & 0 & 0 \\ 0 & 0 & 0 \end{pmatrix}}$$

10 components, 4 independent

$$\sigma^x_{xx} = -\sigma^x_{yy} = -\sigma^y_{yx} = -\sigma^y_{xy},$$
$$\sigma^z_{xy} = -\sigma^z_{yx}, \sigma^y_{zx} = -\sigma^x_{zy}, \sigma^x_{yz} = -\sigma^y_{xz}$$

FeF$_3$
$\mathcal{T}$-odd

$$\overset{\sigma^x}{\begin{pmatrix} \sigma^x_{xx} & 0 & 0 \\ 0 & \sigma^x_{yy} & \sigma^x_{yz} \\ 0 & \sigma^x_{zy} & 0 \end{pmatrix}} \overset{\sigma^y}{\begin{pmatrix} 0 & \sigma^y_{xy} & \sigma^y_{xz} \\ \sigma^y_{yx} & 0 & 0 \\ \sigma^y_{zx} & 0 & 0 \end{pmatrix}} \overset{\sigma^z}{\begin{pmatrix} 0 & \sigma^z_{xy} & 0 \\ \sigma^z_{yx} & 0 & 0 \\ 0 & 0 & 0 \end{pmatrix}}$$

10 components, 4 independent

$$\sigma^x_{xx} = -\sigma^x_{yy} = -\sigma^y_{yx} = -\sigma^y_{xy},$$
$$\sigma^z_{xy} = -\sigma^z_{yx}, \sigma^y_{zx} = -\sigma^x_{zy}, \sigma^x_{yz} = -\sigma^y_{xz}$$

MnSe
$\mathcal{T}$-even

$$\overset{\sigma^x}{\begin{pmatrix} 0 & 0 & 0 \\ 0 & 0 & \sigma^x_{yz} \\ 0 & \sigma^x_{zy} & 0 \end{pmatrix}} \overset{\sigma^y}{\begin{pmatrix} 0 & 0 & \sigma^y_{xz} \\ 0 & 0 & 0 \\ \sigma^y_{zx} & 0 & 0 \end{pmatrix}} \overset{\sigma^z}{\begin{pmatrix} 0 & \sigma^z_{xy} & 0 \\ \sigma^z_{yx} & 0 & 0 \\ 0 & 0 & 0 \end{pmatrix}}$$

6 components, 3 independent

$$\sigma^z_{xy} = -\sigma^z_{yx}, \sigma^y_{zx} = -\sigma^x_{zy}, \sigma^x_{yz} = -\sigma^y_{xz}$$

MnSe
$\mathcal{T}$-odd

$$\overset{\sigma^x}{\begin{pmatrix} 0 & \sigma^x_{xy} & 0 \\ \sigma^x_{yx} & 0 & 0 \\ 0 & 0 & 0 \end{pmatrix}} \overset{\sigma^y}{\begin{pmatrix} \sigma^y_{xx} & 0 & 0 \\ 0 & \sigma^y_{yy} & 0 \\ 0 & 0 & 0 \end{pmatrix}} \overset{\sigma^z}{\begin{pmatrix} 0 & 0 & 0 \\ 0 & 0 & 0 \\ 0 & 0 & 0 \end{pmatrix}}$$

4 components, 1 independent

$$\sigma^y_{yy} = -\sigma^x_{xy} = -\sigma^x_{yx} = -\sigma^y_{xx}$$

S3 Database-level extension to the altermagnet list

To examine the transferability of the symmetry hierarchy discussed in the main text, we extend the same magnetic-point-group (MPG) analysis to the spin-split collinear antiferromagnets listed by Guo *et al.* [S2]. Their material list was obtained from experimentally reported magnetic structures in the MAGNDATA database and contains collinear antiferromagnets that allow momentum-dependent spin splitting in the absence of spin-orbit coupling. Here, we did not recompute the electronic structure or the magnitude of the spin Hall conductivity (SHC) for these compounds. Instead, we used the reported MPGs and magnetic space-group types as symmetry input and determined the allowed $\mathcal{T}$-even and $\mathcal{T}$-odd SHC tensor sectors.

All component labels in this section are given in a canonical MPG coordinate convention with the ordered moment aligned along the canonical z axis, $\boldsymbol{M} \parallel \hat{\boldsymbol{z}}$. The listed tensor components σ_{ij}^{k} therefore refer to this canonical MPG-axis convention. They should not be interpreted as material-specific Cartesian labels before mapping the canonical axes onto the structural setting used for a given compound. This distinction is especially important for monoclinic and rhombohedral systems, where different crystallographic settings may relabel the Cartesian axes. Such relabeling changes the names of the tensor components but not the number of allowed components or the number of independent tensor parameters.

FeF_3 illustrates this distinction. In the representative-material analysis of the main text, FeF_3 is treated as a high-symmetry trigonal reference in which the ordered moment preserves the C_{3z} axis. In the Guo-list mapping, FeF_3 instead follows the reported in-plane Fe-moment configuration, which lowers the ordered-state MPG to $2'/m'$. Thus, the two FeF_3 entries correspond to different moment configurations, with the Guo-list tensor expressed in the canonical MPG frame.

For each MPG, we construct the unitary subgroup H and the antiunitary coset $\mathcal{T} \cdot A$ following the same convention as in Sect. S2. For type-I magnetic space groups, the antiunitary coset is empty, and all MPG operations are treated as unitary. For type-III magnetic space groups, the unprimed operations define H, while the primed operations are assigned to A and appear combined with time reversal. We then impose the linear constraints on the entire 27-dimensional tensor space of σ_{ij}^{k}. The resulting tensor forms are summarized in the following as canonical patterns. Because many compounds share the same MPG and several MPGs generate identical tensor patterns, the component tables are given once at the pattern level and then assigned to the material list.

S3.A Canonical tensor patterns

Table S3 and Table S4 define the canonical tensor patterns that appear in the Guo list. Each pattern contains the allowed components and the symmetry relations among them. When no relation is shown, all listed components are independent.

Table S3 Canonical tensor patterns appearing in the database-level MPG analysis. Component labels are given in the canonical MPG coordinate convention with $\boldsymbol{M} \parallel \hat{z}$.

Pattern	Count	Allowed components	Relations
$\mathcal{P}_1$	27/27	All components σ_{ij}^k with $i, j, k = x, y, z$.	None
$\mathcal{P}_2$	6/6	σ_{yz}^x, σ_{zy}^x, σ_{xz}^y, σ_{zx}^y, σ_{xy}^z, σ_{yx}^z	None
$\mathcal{P}_3$	13/13	σ_{xy}^x, σ_{yx}^x, σ_{yz}^x, σ_{zy}^x, σ_{xx}^y, σ_{xz}^y, σ_{yy}^y, σ_{zx}^y, σ_{zz}^y, σ_{xy}^z, σ_{yx}^z, σ_{yz}^z, σ_{zy}^z	None
$\mathcal{P}_4$	14/14	σ_{xx}^x, σ_{xz}^x, σ_{yy}^x, σ_{zx}^x, σ_{zz}^x, σ_{xy}^y, σ_{yx}^y, σ_{yz}^y, σ_{zy}^y, σ_{xx}^z, σ_{xz}^z, σ_{yy}^z, σ_{zx}^z, σ_{zz}^z	None
$\mathcal{P}_5$	7/7	σ_{xz}^x, σ_{zx}^x, σ_{yz}^y, σ_{zy}^y, σ_{xx}^z, σ_{yy}^z, σ_{zz}^z	None
$\mathcal{P}_6$	7/7	σ_{xy}^x, σ_{yx}^x, σ_{xx}^y, σ_{yy}^y, σ_{zz}^y, σ_{yz}^z, σ_{zy}^z	None

Table S4 Continuation of the canonical tensor patterns. The component labels refer to the same canonical MPG coordinate convention as in Table S3.

Pattern	Count	Allowed components	Relations
$\mathcal{P}_7$	6/3	σ_{yz}^x, σ_{zy}^x, σ_{xz}^y, σ_{zx}^y, σ_{xy}^z, σ_{yx}^z	$\sigma_{yz}^x = -\sigma_{xz}^y$, $\sigma_{zy}^x = -\sigma_{zx}^y$, $\sigma_{xy}^z = -\sigma_{yx}^z$
$\mathcal{P}_8$	6/3	σ_{yz}^x, σ_{zy}^x, σ_{xz}^y, σ_{zx}^y, σ_{xy}^z, σ_{yx}^z	$\sigma_{yz}^x = +\sigma_{xz}^y$, $\sigma_{zy}^x = +\sigma_{zx}^y$, $\sigma_{xy}^z = +\sigma_{yx}^z$
$\mathcal{P}_9$	4/1	σ_{xy}^x, σ_{yx}^x, σ_{xx}^y, σ_{yy}^y	$\sigma_{xy}^x = -\sigma_{yy}^y$, $\sigma_{yx}^x = -\sigma_{yy}^y$, $\sigma_{xx}^y = -\sigma_{yy}^y$
$\mathcal{P}_{10}$	10/4	σ_{xx}^x, σ_{yy}^x, σ_{yz}^x, σ_{zy}^x, σ_{xy}^y, σ_{xz}^y, σ_{yx}^y, σ_{zx}^y, σ_{xy}^z, σ_{yx}^z	$\sigma_{xx}^x = -\sigma_{yx}^y$, $\sigma_{yy}^x = +\sigma_{yx}^y$, $\sigma_{yz}^x = -\sigma_{xz}^y$, $\sigma_{zy}^x = -\sigma_{zx}^y$, $\sigma_{xy}^y = +\sigma_{yx}^y$, $\sigma_{xy}^z = -\sigma_{yx}^z$
$\mathcal{P}_{11}$	10/4	σ_{xy}^x, σ_{yx}^x, σ_{yz}^x, σ_{zy}^x, σ_{xx}^y, σ_{xz}^y, σ_{yy}^y, σ_{zx}^y, σ_{xy}^z, σ_{yx}^z	$\sigma_{xy}^x = -\sigma_{yy}^y$, $\sigma_{yx}^x = -\sigma_{yy}^y$, $\sigma_{yz}^x = -\sigma_{xz}^y$, $\sigma_{zy}^x = -\sigma_{zx}^y$, $\sigma_{xx}^y = -\sigma_{yy}^y$, $\sigma_{xy}^z = -\sigma_{yx}^z$

S3.B MPG-level assignment

Table S5 lists the unitary subgroup H and the antiunitary coset $\mathcal{T}\cdot A$ used for each distinct MPG in the Guo list, together with the resulting canonical $\mathcal{T}$-even and $\mathcal{T}$-odd tensor patterns. The columns $|H|$ and $|A|$ give the number of unitary and antiunitary MPG elements obtained by closing these generators under composition.

We adopt $\boldsymbol{M} \parallel \hat{\boldsymbol{z}}$ throughout. For monoclinic classes (2, $2/m$, $2'/m'$, m'), the unique monoclinic axis (the twofold rotation axis or, equivalently, the normal mirror plane) is taken along $\hat{\boldsymbol{y}}$. The notation used for the symmetry operations in Table S5 is as follows.

- E is the identity operation.
- $\mathcal{I}$ is the spatial inversion, $(x, y, z) \to (-x, -y, -z)$.
- $\mathcal{T}$ is the time-reversal operation, which reverses spin and momentum and flips the sign of any $\mathcal{T}$-odd response.
- $C_{n\alpha}$ denotes the proper rotation by $2\pi/n$ about the axis α. Specifically, C_{2x}, C_{2y}, C_{2z} are twofold rotations about the Cartesian x, y, z axes; C_{3z} and C_{3z}^{-1} are threefold rotations about $\hat{\boldsymbol{z}}$ by $+2\pi/3$ and $-2\pi/3$; C_{4z} and C_{4z}^{-1} are fourfold rotations about $\hat{\boldsymbol{z}}$ by $+\pi/2$ and $-\pi/2$; C_{6z} and C_{6z}^{-1} are sixfold rotations about $\hat{\boldsymbol{z}}$ by $+\pi/3$ and $-\pi/3$.
- m_α denotes a mirror plane perpendicular to the axis α. Specifically, m_x, m_y, m_z are mirrors perpendicular to $\hat{\boldsymbol{x}}$, $\hat{\boldsymbol{y}}$, $\hat{\boldsymbol{z}}$.
- $C_{2[\phi]}$ and $m_{[\phi]}$ denote in-plane operations whose axis lies in the xy plane and makes an angle ϕ (in degrees) with $\hat{\boldsymbol{x}}$. $C_{2[\phi]}$ is a twofold rotation about that in-plane axis, and $m_{[\phi]}$ is a mirror whose normal is the same in-plane axis.
- S_n denotes a rotoinversion (improper rotation): $S_{4z} = m_z\, C_{4z}$ and $S_{4z}^{-1} = m_z\, C_{4z}^{-1}$ are improper fourfold operations; $S_6 = \mathcal{I}\, C_{3z}$ and $S_6^{-1} = \mathcal{I}\, C_{3z}^{-1}$ are improper sixfold operations associated with the $\bar{3}$ axis; $S_3 = m_z\, C_{3z}$ and $S_3^{-1} = m_z\, C_{3z}^{-1}$ are improper threefold operations.
- A prefactor $\mathcal{T}$ in front of any spatial operation g (as in $\mathcal{T}C_{2x}$, $\mathcal{T}m_y$, etc.) denotes the antiunitary operation $\mathcal{T}g$, in which the spatial operation g is combined with time reversal. Such operations appear only in the coset $\mathcal{T}\cdot A$ of type-III MPGs.

These generators are precisely those used in our numerical implementation, so the canonical tensor patterns listed in Table S5 are directly reproduced by the linear-constraint procedure of Sect. S2.C.

S3.C Material-level mapping

The material-level mapping is summarized in Tables S6 and S7. Since the tensor forms are already defined at the pattern level, the material table reports only the MPG, the MSG type, the corresponding canonical tensor patterns and the allowed/independent component counts.

The survey confirms that the separation between the two SHC channels is not specific to the six representative materials discussed in the main text. For type-I MPGs, the antiunitary coset is absent, and therefore the $\mathcal{T}$-even and $\mathcal{T}$-odd tensor spaces have the same canonical tensor pattern. This is seen, for example, in the entries mmm, $2/m$, $4/mmm$, $\bar{3}m$, and $3m$. By contrast, type-III MPGs can distinguish the two channels because operations in the antiunitary coset act with opposite signs in $\mathcal{T}$-even and $\mathcal{T}$-odd responses. This produces distinct tensor patterns in $2'/m'$, m', $m'm'm$, $m'm2'$, $4'/mm'm$, and $6'/m'mm'$.

Several trends are apparent at the MPG level. Low-symmetry centrosymmetric classes such as $\bar{1}$ leave all 27 SHC components allowed. Monoclinic classes such as $2/m$ and $2'/m'$ allow large tensor spaces with 13 or 14 independent components depending on the time-reversal parity. Higher rotational symmetries strongly reduce the tensor rank. The tetragonal and hexagonal patterns contain only six allowed $\mathcal{T}$-even components with three independent parameters, while the $\mathcal{T}$-odd sector of $6'/m'mm'$ is reduced to four allowed components with only one independent parameter. Thus, the Guo-list extension provides a symmetry prescreening map for identifying which MPG classes can host a desired SHC tensor sector before performing dense first-principles transport calculations.

Table S5 lists the operation sets or generating sets used to construct H and $\mathcal{T}\cdot A$.

MPG	MSG type	$\|H\|$	$\|A\|$	H	$\mathcal{T}\cdot A$	$\mathcal{T}$-even	$\mathcal{T}$-odd
$\bar{1}$	I	2	0	E, $\mathcal{I}$	—	$\mathcal{P}_1$	$\mathcal{P}_1$
2	I	2	0	E, C_{2y}	—	$\mathcal{P}_3$	$\mathcal{P}_3$
$2/m$	I	4	0	E, C_{2y}, $\mathcal{I}$, m_y	—	$\mathcal{P}_3$	$\mathcal{P}_3$
$mm2$	I	4	0	E, C_{2z}, m_x, m_y	—	$\mathcal{P}_2$	$\mathcal{P}_2$
mmm	I	8	0	E, C_{2x}, C_{2y}, C_{2z}, $\mathcal{I}$, m_x, m_y, m_z	—	$\mathcal{P}_2$	$\mathcal{P}_2$
$\bar{4}2m$	I	8	0	E, C_{2z}, S_{4z}, S_{4z}^{-1}, C_{2x}, C_{2y}, $m_{[45]}$, $m_{[135]}$	—	$\mathcal{P}_7$	$\mathcal{P}_7$
$4/mmm$	I	16	0	closure of $\{C_{4z}, C_{2x}, \mathcal{I}\}$	—	$\mathcal{P}_7$	$\mathcal{P}_7$
$3m$	I	6	0	E, C_{3z}, C_{3z}^{-1}, $m_{[90]}$, $m_{[210]}$, $m_{[330]}$	—	$\mathcal{P}_{11}$	$\mathcal{P}_{11}$
$\bar{3}m$	I	12	0	E, C_{3z}, C_{3z}^{-1}, $\mathcal{I}$, S_6, S_6^{-1}, $C_{2[0]}$, $C_{2[120]}$, $C_{2[240]}$, $m_{[0]}$, $m_{[120]}$, $m_{[240]}$	—	$\mathcal{P}_{10}$	$\mathcal{P}_{10}$
m'	III	1	1	E	$\mathcal{T}m_y$	$\mathcal{P}_3$	$\mathcal{P}_4$
$2'/m'$	III	2	2	E, $\mathcal{I}$	$\mathcal{T}C_{2y}$, $\mathcal{T}m_y$	$\mathcal{P}_3$	$\mathcal{P}_4$
$2'2'2$	III	2	2	E, C_{2z}	$\mathcal{T}C_{2x}$, $\mathcal{T}C_{2y}$	$\mathcal{P}_2$	$\mathcal{P}_5$
$m'm2'$	III	2	2	E, m_y	$\mathcal{T}C_{2z}$, $\mathcal{T}m_x$	$\mathcal{P}_2$	$\mathcal{P}_6$
$m'm'2$	III	2	2	E, C_{2z}	$\mathcal{T}m_x$, $\mathcal{T}m_y$	$\mathcal{P}_2$	$\mathcal{P}_5$
$m'm'm$	III	4	4	E, C_{2z}, $\mathcal{I}$, m_z	$\mathcal{T}C_{2x}$, $\mathcal{T}C_{2y}$, $\mathcal{T}m_x$, $\mathcal{T}m_y$	$\mathcal{P}_2$	$\mathcal{P}_5$
$4'/mm'm$	III	8	8	E, C_{2x}, C_{2y}, C_{2z}, $\mathcal{I}$, m_x, m_y, m_z	$\mathcal{T}C_{4z}$, $\mathcal{T}C_{4z}^{-1}$, $\mathcal{T}S_{4z}$, $\mathcal{T}S_{4z}^{-1}$, $\mathcal{T}C_{2[45]}$, $\mathcal{T}C_{2[135]}$, $\mathcal{T}m_{[45]}$, $\mathcal{T}m_{[135]}$	$\mathcal{P}_7$	$\mathcal{P}_8$
$6'/m'mm'$	III	12	12	E, C_{3z}, C_{3z}^{-1}, $\mathcal{I}$, S_6, S_6^{-1}, $C_{2[30]}$, $C_{2[90]}$, $C_{2[150]}$, $m_{[30]}$, $m_{[90]}$, $m_{[150]}$	$\mathcal{T}C_{6z}$, $\mathcal{T}C_{6z}^{-1}$, $\mathcal{T}C_{2z}$, $\mathcal{T}S_3$, $\mathcal{T}S_3^{-1}$, $\mathcal{T}m_z$, $\mathcal{T}C_{2[0]}$, $\mathcal{T}C_{2[60]}$, $\mathcal{T}C_{2[120]}$, $\mathcal{T}m_{[0]}$, $\mathcal{T}m_{[60]}$, $\mathcal{T}m_{[120]}$	$\mathcal{P}_7$	$\mathcal{P}_9$

Table S6 Material-level mapping for entries 1–31 of the Guo altermagnet list. Metallic compounds are marked by *, following Ref. [S2]. When the same chemical formula appears more than once, the parenthesized number denotes the corresponding entry number in the Guo list.

No.	Compound	MPG	Type	$\mathcal{T}$-even	$\mathcal{T}$-odd	Count even/odd
1	$BaCrF_5$	$2'2'2$	III	$\mathcal{P}_2$	$\mathcal{P}_5$	6/6, 7/7
2	$LaCrO_3$ (#2)	mmm	I	$\mathcal{P}_2$	$\mathcal{P}_2$	6/6, 6/6
3	$ScCrO_3$	mmm	I	$\mathcal{P}_2$	$\mathcal{P}_2$	6/6, 6/6
4	$InCrO_3$	mmm	I	$\mathcal{P}_2$	$\mathcal{P}_2$	6/6, 6/6
5	$TlCrO_3$	mmm	I	$\mathcal{P}_2$	$\mathcal{P}_2$	6/6, 6/6
6	$TbCrO_3$	$m'm'm$	III	$\mathcal{P}_2$	$\mathcal{P}_5$	6/6, 7/7
7	$LaCrO_3$ (#7)	$m'm'm$	III	$\mathcal{P}_2$	$\mathcal{P}_5$	6/6, 7/7
8	$YCrO_3$	$m'm'm$	III	$\mathcal{P}_2$	$\mathcal{P}_5$	6/6, 7/7
9	$CrNb_4S_8^*$	$6'/m'mm'$	III	$\mathcal{P}_7$	$\mathcal{P}_9$	6/3, 4/1
10	$CrSb^*$	$6'/m'mm'$	III	$\mathcal{P}_7$	$\mathcal{P}_9$	6/3, 4/1
11	$RbMnF_4$	$\bar{1}$	I	$\mathcal{P}_1$	$\mathcal{P}_1$	27/27, 27/27
12	$MnTiO_3$	m'	III	$\mathcal{P}_3$	$\mathcal{P}_4$	13/13, 14/14
13	$MnCO_3$	$2/m$	I	$\mathcal{P}_3$	$\mathcal{P}_3$	13/13, 13/13
14	$Ca_3Mn_2O_7$	$m'm2'$	III	$\mathcal{P}_2$	$\mathcal{P}_6$	6/6, 7/7
15	$SrMn_2V_2O_8$	$m'm2'$	III	$\mathcal{P}_2$	$\mathcal{P}_6$	6/6, 7/7
16	$Mn(N(CN)_2)_2$	$m'm'm$	III	$\mathcal{P}_2$	$\mathcal{P}_5$	6/6, 7/7
17	$LaMnO_3$	$m'm'm$	III	$\mathcal{P}_2$	$\mathcal{P}_5$	6/6, 7/7
18	$Mn_2SeO_3F_2$	$m'm'm$	III	$\mathcal{P}_2$	$\mathcal{P}_5$	6/6, 7/7
19	$Ba_2MnSi_2O_7$	$\bar{4}2m$	I	$\mathcal{P}_7$	$\mathcal{P}_7$	6/3, 6/3
20	$ZrMn_2Ge_4O_{12}$	$4'/mm'm$	III	$\mathcal{P}_7$	$\mathcal{P}_8$	6/3, 6/3
21	MnF_2	$4'/mm'm$	III	$\mathcal{P}_7$	$\mathcal{P}_8$	6/3, 6/3
22	$KMnF_3$	$4/mmm$	I	$\mathcal{P}_7$	$\mathcal{P}_7$	6/3, 6/3
23	Fe_2O_3 (#23)	$\bar{1}$	I	$\mathcal{P}_1$	$\mathcal{P}_1$	27/27, 27/27
24	$LiFeP_2O_7$	2	I	$\mathcal{P}_3$	$\mathcal{P}_3$	13/13, 13/13
25	$Fe_3(PO_4)_2(OH)_2$	$2/m$	I	$\mathcal{P}_3$	$\mathcal{P}_3$	13/13, 13/13
26	$FeSO_4F$	$2'/m'$	III	$\mathcal{P}_3$	$\mathcal{P}_4$	13/13, 14/14
27	$FeOHSO_4$	$2'/m'$	III	$\mathcal{P}_3$	$\mathcal{P}_4$	13/13, 14/14
28	FeF_3	$2'/m'$	III	$\mathcal{P}_3$	$\mathcal{P}_4$	13/13, 14/14
29	$FeBO_3$	$2'/m'$	III	$\mathcal{P}_3$	$\mathcal{P}_4$	13/13, 14/14
30	Fe_2O_3 (#30)	$2'/m'$	III	$\mathcal{P}_3$	$\mathcal{P}_4$	13/13, 14/14
31	$ZnFeF_5(H_2O)_2$	$mm2$	I	$\mathcal{P}_2$	$\mathcal{P}_2$	6/6, 6/6

Table S7 Material-level mapping for entries 32–62 of the Guo altermagnet list.

No.	Compound	MPG	Type	$\mathcal{T}$-even	$\mathcal{T}$-odd	Count even/odd
32	Fe_2PO_5	mmm	I	$\mathcal{P}_2$	$\mathcal{P}_2$	6/6, 6/6
33	$SmFeO_3$ (#33)	$m'm'm$	III	$\mathcal{P}_2$	$\mathcal{P}_5$	6/6, 7/7
34	$NdFeO_3$	$m'm'm$	III	$\mathcal{P}_2$	$\mathcal{P}_5$	6/6, 7/7
35	$TbFeO_3$	$m'm'm$	III	$\mathcal{P}_2$	$\mathcal{P}_5$	6/6, 7/7
36	$SmFeO_3$ (#36)	$m'm'm$	III	$\mathcal{P}_2$	$\mathcal{P}_5$	6/6, 7/7
37	$Sr_4Fe_4O_{11}$	$m'm'm$	III	$\mathcal{P}_2$	$\mathcal{P}_5$	6/6, 7/7
38	$LiFe_2F_6$	$4'/mm'm$	III	$\mathcal{P}_7$	$\mathcal{P}_8$	6/3, 6/3
39	$FeCO_3$	$\bar{3}m$	I	$\mathcal{P}_{10}$	$\mathcal{P}_{10}$	10/4, 10/4
40	Sr_2CoTeO_6	$2/m$	I	$\mathcal{P}_3$	$\mathcal{P}_3$	13/13, 13/13
41	$Li_2Co(SO_4)_2$	$2'/m'$	III	$\mathcal{P}_3$	$\mathcal{P}_4$	13/13, 14/14
42	$Ba_2CoGe_2O_7$	$m'm2'$	III	$\mathcal{P}_2$	$\mathcal{P}_6$	6/6, 7/7
43	CoF_2	$4'/mm'm$	III	$\mathcal{P}_7$	$\mathcal{P}_8$	6/3, 6/3
44	CoF_3	$\bar{3}m$	I	$\mathcal{P}_{10}$	$\mathcal{P}_{10}$	10/4, 10/4
45	$NiCO_3$	$2/m$	I	$\mathcal{P}_3$	$\mathcal{P}_3$	13/13, 13/13
46	La_2NiO_4	$m'm'm$	III	$\mathcal{P}_2$	$\mathcal{P}_5$	6/6, 7/7
47	NiF_2	$m'm'm$	III	$\mathcal{P}_2$	$\mathcal{P}_5$	6/6, 7/7
48	$NiFePO_5$	mmm	I	$\mathcal{P}_2$	$\mathcal{P}_2$	6/6, 6/6
49	$PbNiO_3$	$3m$	I	$\mathcal{P}_{11}$	$\mathcal{P}_{11}$	10/4, 10/4
50	$Y_2Cu_2O_5$	$mm2$	I	$\mathcal{P}_2$	$\mathcal{P}_2$	6/6, 6/6
51	$Cu_2V_2O_7$	$m'm'2$	III	$\mathcal{P}_2$	$\mathcal{P}_5$	6/6, 7/7
52	$CuFePO_5$	mmm	I	$\mathcal{P}_2$	$\mathcal{P}_2$	6/6, 6/6
53	Ca_3LiRuO_6	$2'/m'$	III	$\mathcal{P}_3$	$\mathcal{P}_4$	13/13, 14/14
54	Sr_3LiRuO_6	$2'/m'$	III	$\mathcal{P}_3$	$\mathcal{P}_4$	13/13, 14/14
55	RuO_2^*	$4'/mm'm$	III	$\mathcal{P}_7$	$\mathcal{P}_8$	6/3, 6/3
56	$Ba_3NiRu_2O_9$	$6'/m'mm'$	III	$\mathcal{P}_7$	$\mathcal{P}_9$	6/3, 4/1
57	K_2ReI_6	$2/m$	I	$\mathcal{P}_3$	$\mathcal{P}_3$	13/13, 13/13
58	Sr_2CoOsO_6	$2/m$	I	$\mathcal{P}_3$	$\mathcal{P}_3$	13/13, 13/13
59	Ca_3LiOsO_6	$2'/m'$	III	$\mathcal{P}_3$	$\mathcal{P}_4$	13/13, 14/14
60	$NaOsO_3$	$m'm'm$	III	$\mathcal{P}_2$	$\mathcal{P}_5$	6/6, 7/7
61	$Ba_3CoIr_2O_9$	$2/m$	I	$\mathcal{P}_3$	$\mathcal{P}_3$	13/13, 13/13
62	$CaIrO_3$	$m'm'm$	III	$\mathcal{P}_2$	$\mathcal{P}_5$	6/6, 7/7

References

[S1] Roy, A., Guimarães, M.H., Sławińska, J.: Unconventional spin Hall effects in nonmagnetic solids. Phys. Rev. Mater. **6**(4), 045004 (2022)

[S2] Guo, Y., Liu, H., Janson, O., Fulga, I.C., Brink, J., Facio, J.I.: Spin-split collinear antiferromagnets: A large-scale ab-initio study. Mater. Today Phys. **32**, 100991 (2023)